
Since January 2020 Elsevier has created a COVID-19 resource centre with free information in English and Mandarin on the novel coronavirus COVID-19. The COVID-19 resource centre is hosted on Elsevier Connect, the company's public news and information website.

# Tropism of Severe Acute Respiratory Syndrome Coronavirus 2 for Barrett's Esophagus May Increase Susceptibility to Developing Coronavirus Disease 2019

**Ramon U. Jin**,[1,*] **Jeffrey W. Brown**,[2,*] Qing Kay Li,[3] Peter O. Bayguinov,[4] Jean S. Wang,[2] and Jason C. Mills[2,5,6]

*[1]Division of Oncology, Department of Medicine, Washington University in St Louis, School of Medicine, St Louis, Missouri; [2]Division of Gastroenterology, Department of Medicine, Washington University in St Louis, School of Medicine, St Louis, Missouri; [3]Department of Pathology, Johns Hopkins Medical Institutions, Baltimore, Maryland; [4]Washington University Center for Cellular Imaging, Washington University School of Medicine, St Louis, Missouri; [5]Department of Pathology and Immunology, Washington University in St Louis, School of Medicine, St Louis, Missouri; and [6]Department of Developmental Biology, Washington University in St Louis, School of Medicine, St Louis, Missouri*

Coronavirus disease 2019 (COVID-19), caused by severe acute respiratory syndrome coronavirus 2 (SARS-CoV-2), is a global pandemic, spurring the exigent need for determining how the virus is transmitted and what increases disease susceptibility.

Gastrointestinal (GI) symptoms are prominent in COVID-19, and live virus is detected along the GI tract and in stool.[1] SARS-CoV-2 enters host cells via its transmembrane spike glycoproteins that bind host angiotensin-converting enzyme 2 (ACE-2) protein on the cell surface, an interaction facilitated by spike protein cleavage catalyzed by host type II transmembrane serine protease (TMPRSS2).[2] Thus, concurrent cellular expression of ACE-2 and TMPRSS2 determines cellular tropism for SARS-CoV-2. Surveys of ACE-2 and TMPRSS2 in GI tissues have shown abundant expression in human intestines.[3] However, the low pH of gastric secretions[4] and the emulsifying conditions[3] of the small and large intestines inactivate the virus, limiting access of infective virus to distal GI tissues via the GI tract lumen.

Here, we show that individuals with intestinal metaplasia (ie, ectopic intestine-like cells in their esophagus as in Barrett's esophagus) would have increased potential for viable, ingested virus to interact with a receptive host epithelium. Thus, intestinal metaplasia could present a previously unappreciated orogastric route for viral entry in individuals with this condition.

## Methods

All human tissue blocks were collected from the archives of The Johns Hopkins School of Medicine Bayview Medical Campus Department of Pathology. Barrett's esophagus organoids were derived from deidentified tissue from patients who were undergoing surveillance esophagogastroduodenoscopy for previously identified nondysplastic Barrett's esophagus and who provided informed consent through the Washington University School of Medicine Digestive Disease Research Core Center. Human tissue collection was approved by the review boards of each institution. Organoid cultures were infected with a chimeric virus expressing the SARS-CoV-2 spike protein (recombinant vesicular stomatitis virus [rVSV]–enhanced green fluorescent protein [eGFP]–SARS-CoV-2). Both fixed and live cells were imaged by light, epifluorescence, and live confocal microscopy.

## Results

To test whether intestinal-type metaplasias of the proximal GI foregut might be receptive to SARS-CoV-2 infection, we determined ACE-2 and TMPRSS2 expression in a series of esophageal and gastric biopsies harboring intestinal metaplasia (Supplementary Table 1). Unlike normal esophageal and gastric tissue, intestinal-type metaplasia of the esophagus and stomach strongly expressed both ACE-2 and TMPRSS2 on epithelial cells with ACE-2 predominantly localized to the apical plasma membranes (Figure 1*A*, Supplementary Figure 1A, and Supplementary Table 1). The findings were corroborated by analyses of previous global surveys of RNA expression[5] showing that unlike normal esophageal and gastric tissue, intestinal-type metaplasias of these tissues aberrantly express *ACE2* and *TMPRSS2* messenger RNA.

To test whether Barrett's metaplasia is susceptible to infection by SARS-CoV-2, we chose an ex vivo model: organoids derived from patients with Barrett's esophagus. We first demonstrated that organoids generated from biopsies of Barrett's esophagus faithfully reproduce the in vivo histopathologic characteristics (Supplementary Figure 1*B*). Specifically, they form a columnar monolayer that is low in expression of the foregut transcription factor SOX2, high in expression of the mid and hindgut transcription factor CDX2, reactive to the histochemical goblet cell mucin stain

***Authors share co-first authorship.**

***Abbreviations used in this paper:*** **ACE-2, angiotensin-converting enzyme 2; COVID-19, coronavirus disease 2019; eGFP, enhanced green fluorescent protein; GI, gastrointestinal; rVSV, recombinant vesicular stomatitis virus; SARS-CoV-2, severe acute respiratory syndrome coronavirus 2; TMPRSS2, transmembrane protease, serine 2; VSV, vesicular stomatitis virus.**

**Most current article**


0016-5085/$36.00
https://doi.org/10.1053/j.gastro.2021.01.024

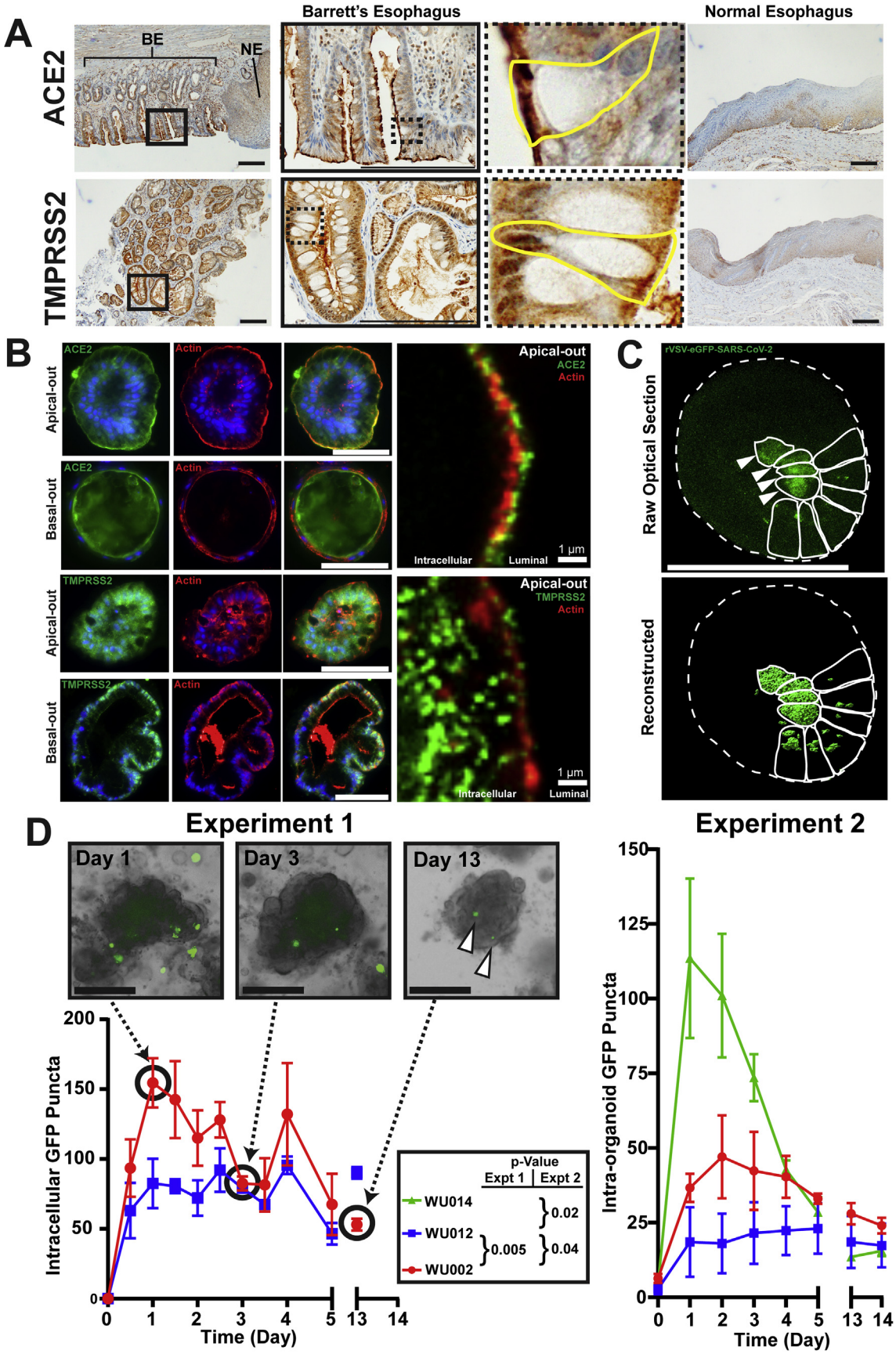
A
Barrett's Esophagus
Normal Esophagus
ACE2
TMPRSS2
BE
NE
B
Apical-out
Basal-out
ACE2
Actin
TMPRSS2
Intracellular
Luminal
1 μm
C
rVSV-eGFP-SARS-CoV-2
Raw Optical Section
Reconstructed
D
Experiment 1
Experiment 2
Day 1
Day 3
Day 13
Intracellular GFP Puncta
Intra-organoid GFP Puncta
Time (Day)
p-Value
Expt 1
Expt 2
WU014
WU012
WU002
0.02
0.005
0.04

Alcian blue, and, importantly for this study, maintain the apical expression of ACE-2 and TMPRSS2 (Figure 1*B* and Supplementary Figure 1*B* and *C*).

We incubated 3 Barrett's esophageal organoid lines (WU014, WU002, and WU012) harboring unique intestinal characteristics (Supplementary Figure 1*B*) with a chimeric virus (rVSV–eGFP–SARS-CoV-2) in which the SARS-CoV-2 spike protein replaces the VSV glycoprotein G and the eGFP gene is carried within viral RNA to report on intracellular translation of viral proteins. Thus, this chimeric virus exhibits the same tropism and cell invasion behavior of actual SARS-CoV-2 but can be studied in a Biosafety Level 2 facility. rVSV–eGFP–SARS-CoV-2 infected cells within 12 hours, and the GFP signal, indicating active translation of viral RNA, persisted until our last time point 2 weeks later (Figure 1*C* and *D*; Supplementary Figure 1*D*). We observed in an initial experiment (Experiment 1, Figure 1*D*) that although both patient organoid lines were efficiently infected, the line with increased intestinalization (ie, lower SOX2-to-CDX2 ratio; Supplementary Figure 1*B*) was more extensively infected. We thus repeated the experiment (Experiment 2, Figure 1*D*)but added an additional line (WU0014) featuring even greater intestinal features (Supplementary Figure 1*B*). In Experiment 2, we also reasoned virus in patients would encounter intact epithelium, so we scored only those infected cells within organoids above a threshold size. Together, these organoid results show that Barrett's esophagus may serve as a novel in vivo niche for SARS-CoV-2 and that viral entry may increase with increasing intestinalization (Figure 1*D*).

## Discussion

Esophageal and gastric metaplasia are caused by chronic injury and predispose individuals to developing adenocarcinoma of the respective tissue.[6,7] However, the data presented here suggest that these metaplasias may also have other unanticipated consequences.

We show that intestinal-type metaplasia of the esophagus and stomach aberrantly express the proteins critical for binding and invasion by SARS-CoV-2: ACE-2 and TMPRSS2. Recent studies have demonstrated that the low pH of the stomach and the luminal fluid of the small and large intestines greatly attenuate the infectivity of SARS-CoV-2 that is present in swallowed oral secretions and refluxed respiratory sputum.[3,4] Thus, the ectopic, proximal expression of ACE-2 and TMPRSS2 may become salient because it means host receptors for SARS-CoV-2 are located in a region of the digestive tract where higher viable viral titers exist after ingestion. Moreover, individuals with known Barrett's esophagus are almost universally treated with proton pump inhibitors, and those with gastric intestinal metaplasia almost invariably have loss of acid-secreting parietal cells.[6,7] Thus, the decreased ability for the stomach to produce acid either by pharmacologic inhibition or loss of acid-secreting cells may compound the risk due to increased gastric pH that could result in increased viral titers and prolonged exposure. In addition, epidemiologically, intestinal metaplasia increases with age and male sex, paralleling demographics of those most susceptible to COVID-19.[8]

Previous work indicated that viable virus infects cells via SARS-CoV-2 spike protein interaction with apical ACE-2 receptor. Two factors in our cultures increased apical exposure of cells to virus: (1) we administered virus immediately after passaging (ie, after dissociating organoids to single cells exposing all cell surfaces), and (2) as new Barrett's organoids form, many wholly or partially orient "apical-out," that is, with cell apices exposed to the culture medium (Figure 1*B*). Importantly, all 3 organoid lines had equivalent distribution of apical-out, basal-out, and hybrid orientations (data not shown) indicating orientation did not affect infectivity.

**Figure 1.** Barrett's esophagus expresses ACE-2 and TMPRSS2 and is readily infected by rVSV–eGFP–SARS-CoV-2. (*A*) Human Barrett's esophagus immunohistochemistry shows expression of apical ACE-2, the host receptor for the SARS-CoV-2 spike protein, and TMPRSS2, the necessary protease. Insets highlight individual goblet cells outlined in yellow with apical ACE-2 and TMPRSS2 expression patterns. Normal esophagus does not express apical ACE-2 or TMPRSS2. Scale bars, 200 $\mu$m. BE, area of Barrett's esophagus; NE, adjacent area of normal squamous esophagus. (*B*) Barrett's organoids grow with various mixtures of "apical-out" and "basal-out" arrangements. Epifluorescence imaging of fixed organoids demonstrates apical ACE-2 staining (*green*) and TMPRSS2 staining (*green*) with $\beta$-actin staining (*red*) highlighting the apical surface. Confocal imaging using an Airyscan detector in SR mode showing super-resolution co-localization of ACE-2 (*green*) and TMPRSS2 (*green*) with apical $\beta$-actin (*red*); intracellular and luminal spaces are highlighted. Scale bars, 100 $\mu$m or as indicated. (*C*) Z-stack still image of live confocal microscopy of infected Barrett's organoids with raw optical section and 3-dimensional reconstruction shown. Organoid outer surface marked by *dotted line*, and individual green infected cells are outlined with a *solid line* in each organoid, showing diffuse cytoplasmic (*arrowheads*) and punctate vesicular GFP patterns. Scale bars, 100 $\mu$m. (*D*) Incubation of Barrett's esophagus organoids (WU014 with mostly intestinal features, WU002 with mixed intestinal–gastric features, and WU012 with mostly gastric features; see Supplementary Figure 1*B*) with rVSV–eGFP–SARS-CoV-2. Experiment 1: quantification of all intracellular punctate GFP foci in Barrett's organoids (2 independent cultures); Experiment 2: only GFP puncta within organoids $>$ 10 $\mu$m scored (3–6 independent cultures) at specified time points for 2 weeks. Live-cell brightfield and fluorescence imaging of WU002 Barrett's organoids at time points indicated. Note: A single field of organoids is followed serially in each panel. Persistently infected (green from GFP translated from rVSV–eGFP–SARS-CoV-2 virus) cells are indicated at the day 13 time point (*arrowheads*). Scale bars, 200 $\mu$m. *P*-values by 2-tailed, paired Student's *t* test (Experiment 1) and by analysis of variance with Dunnett multiple comparison test to WU012 as control (Experiment 2) of the area under the curve at each time point from the first time point to day 5 (see Supplementary Methods).

Overall, our data suggest that individuals with intestinal-type metaplasias of the proximal GI tract (eg, Barrett's esophagus, in particular) are potentially at higher risk for developing or experiencing a more severe presentation of COVID-19 relative to the general population. Future studies to determine the additional risk posed by ectopic proximal expression of ACE-2 and TMPRSS2 should include infection of a much broader panel of organoids of varying intestinal differentiation and, eventually, large-scale retrospective database analyses correlated with autopsy series to analyze COVID-19 outcome vs viral load and extent of metaplasia.

## Supplementary Material

Note: To access the supplementary material accompanying this article, visit the online version of *Gastroenterology* at www.gastrojournal.org, and at https://doi.org/10.1053/j.gastro.2021.01.024.

## References


1. Xiao F, et al. Gastroenterology 2020;158:1831–1833.
2. Hoffman M, et al. Cell 2020;181:271–280.
3. **Zang R, Castro MFG**, et al. Sci Immunol 2020;5:eabc3582.
4. **Zang R, Castro MFG**, et al. BioRXiv 2020.
5. di Pietro M, et al. Proc Natl Acad Sci 2012;109:9077–9082.
6. Spechler SJ, et al. N Engl J Med 2014;371:836–845.
7. Amieva M, et al. Gastroenterology 2016;150:64–78.
8. Wu Z, et al. JAMA 2020;323:1239–1242.


**Author names in bold are co–first authors.**

**Received September 3, 2020. Accepted January 10, 2021.**

**Correspondence**
Address correspondence to: Jason C. Mills, MD, PhD, Washington University in St Louis, School of Medicine, 660 South Euclid Avenue, Campus Box 8124, St Louis, MO 63110. e-mail: jmills@wustl.edu; or Jeffrey W. Brown, M.D., Ph.D. Washington University in St. Louis, School of Medicine 660 S. Euclid Avenue, Campus Box 8124 St. Louis, MO 63110. e-mail: brownjw@wustl.edu.

**Acknowledgments**
The authors thank Sean P. J. Whelan, PhD, and James A. J. Fitzpatrick, PhD, from the Washington University School of Medicine, St Louis, and Alan K. Meeker, MAT, PhD, from the Johns Hopkins Medical Institutions, Baltimore, for their collaboration on this article.

**CRediT Authorship Contributions**
Ramon U. Jin, MD, PhD (Conceptualization: Equal). Jeffrey W. Brown, MD, PhD (Writing – original draft: Equal). Qing Kay Li, MD, PhD (Investigation: Supporting). Peter O. Bayguinov, PhD (Investigation: Supporting). Jean S. Wang, MD, PhD (Resources: Supporting). Jason C Mills, MD, PhD (Conceptualization: Equal; Investigation: Supporting; Resources: Equal; Supervision: Lead).

**Conflicts of interest**
The authors disclose no conflicts.

**Funding**
This study was supported by the American Gastroenterological Association Foundation AGA-Takeda COVID-19 Rapid Response Research Award AGA2021-5101 and the Department of Defense through the Peer Reviewed Cancer Research Program (PRCRP) program under award no. W81XWH-20-1-0630 to Jeffrey W. Brown; the Washington University Center for Cellular Imaging (supported by Washington University School of Medicine), the Children's Discovery Institute of Washington University and St Louis Children's Hospital (CDI-CORE-2015-505 and CDI-CORE-2019-813), the Foundation for Barnes-Jewish Hospital (3770 and 4642), and the Alvin J. Siteman Cancer Center at Barnes-Jewish Hospital and Washington University School of Medicine (P30 CA091842) to Peter O. Bayguinov and James A. J. Fitzpatrick (collaborator); the Advanced Imaging and Tissue Analysis Core of the Washington University Digestive Disease Research Core Center (P30 DK052574) and the Oncology Tissue Core at JHU (P30 CA006973); grant T32HL007088 to Ramon U. Jin; the BETRNet (NCI U54CA163060) to Ramon U. Jin and Jason C. Mills; and NIH grants R21DK111369, R01DK105129, and R01DK110406 to Jason C. Mills.

# Supplementary Methods

## Human Sample Collection, Immunohistochemistry, and Quantification

Formalin-fixed paraffin-embedded tissue blocks of the esophagus (n = 26) and stomach (n = 5) were from The Johns Hopkins School of Medicine Bayview Medical Campus Department of Pathology with Institutional Review Board approval. Formalin-fixed paraffin-embedded blocks were cut into 4-$\mu$m sections, deparaffinized, and rehydrated before incubation with primary antibodies.

For manual ACE-2 immunostaining, heat-induced antigen retrieval was via a steamer using Antigen Unmasking Solution (H-3300; Vector Laboratories) with blocking of endogenous peroxidase and phosphatase (S2003; Dako). Anti-ACE2 (1:2000 dilution, Ab15348; Abcam) was detected by horseradish peroxidase (HRP)-labeled anti-rabbit secondary antibody (PV6119; Leica Microsystems), visualized with 3,3′-diaminobenzidine (D4293; Sigma-Aldrich), and counterstained with Mayer's hematoxylin. ACE-2 autostaining used a Ventana Discovery Ultra autostainer (Roche Diagnostics) with antigen retrieval performed by Ventana Ultra CC1 buffer (no. 6414575001; Roche Diagnostics). Primary antibody was detected with an anti-rabbit HQ detection system (nos. 7017936001 and 7017812001; Roche), visualized with the Chromomap DAB IHC detection kit (no. 5266645001; Roche) and counterstained with hematoxylin. For TMPRSS2 immunostaining, autostaining was done as above with anti-TMPRSS2 (1:12,000 dilution, Ab92323; Abcam) primary antibody detected with the same anti-rabbit HQ detection system (nos. 7017936001 and 7017812001; Roche), visualized by the Chromomap DAB IHC kit (no. 5266645001; Roche Diagnostics), and counterstained with hematoxylin.

ACE2 and TMPRSS2 staining were quantified in areas of Barrett's esophagus or gastric intestinal metaplasia through review of hematoxylin and eosin histology. ACE-2 and TMPRSS2 stained serial sections were scored as follows: 0 = no apical staining; 1 = <50% of apical staining, 2 = >50% apical staining in 20× fields of view in areas of Barrett's esophagus or gastric intestinal metaplasia and adjacent tissue controls when available.

## Human Barrett's Esophagus Organoid Culture System

Barrett's esophagus organoids were derived from deidentified tissue from patients who were undergoing Barrett's esophagus surveillance esophagogastroduodenoscopy for previously identified nondysplastic Barrett's esophagus, approved by the Institutional Review Board of Washington University School of Medicine, and who provided informed consent through the Washington University School of Medicine Digestive Disease Research Core Center. In brief, Barrett's esophagus organoids were cultured with L-WRN-conditioned media[1] supplemented with 10 nM gastrin (Sigma-Aldrich), 10 mM nicotinamide (Sigma-Aldrich), 500 nM A83-01 (Tocris), 10 $\mu$M SB202190 (Sigma-Aldrich), 200 ng/mL FGF10 (Peprotech), 10 $\mu$M Y-27632 (Sigma-Aldrich), and Primocin (Invivogen) in 3D Matrigel (Corning) in 24-well plates.[2] Organoids were expanded and passaged every 7–10 days (except for virus infection experiments, see below) by mechanical dissociation from Matrigel, dispersed using TrypLE (Thermo Fisher) and manual pipetting, and transferred into new Matrigel and plated in 24-well plates.

## Human Barrett's Esophagus Organoid Immunofluorescence/Immunohistochemical Staining

Human Barrett's esophagus organoids were pelleted and fixed in 10% formalin at 4°C for 1 hour. Organoids were washed, moved to 70% ethanol, mounted in 3% agar, and embedded in paraffin. Blocks were cut into 7-$\mu$m sections. For immunofluorescence, tissue microtome sections underwent a standard deparaffinization with xylene and rehydration protocol and were antigen retrieved in sodium citrate buffer (2.94 g sodium citrate, 500 $\mu$L Tween 20, pH 6.0) using a pressure cooker. Sections were blocked in 1% bovine serum albumin, 0.3% Triton X-100 in phosphate-buffered saline, and incubated with primary antibodies: anti-ACE-2 (1:100 dilution, catalog no. Ab15348; Abcam), anti-TMPRSS2 (1:100 dilution, catalog no. HPA035787; Sigma-Aldrich), and anti-$\beta$-Actin (1:200 dilution, catalog no. A1978; Sigma-Aldrich). Fluorescent secondary antibodies were applied, and slides were mounted using ProLong Gold antifade reagent with DAPI (Molecular Probes). For immunohistochemistry, the same manual staining procedure for anti-ACE-2 staining and autostaining procedure for TMPRSS2 was used as described above.

## Viral Infection of Human Barrett's Esophagus Organoids and Quantification

rVSV–eGFP–SARS-CoV-2 chimeric virus (eGFP reporter encoded in the viral RNA) was constructed by 2 collaborating authors (P.W. Rothlauf and S.P.J. Whelan) using the SARS-CoV-2 Wuhan-Hu-1 spike and the VSV Indiana strain.[3] The virus was generated and recovered according to previous published methods[4] and propagated in MA104 cells (ATCC). Organoids were infected with $2.0 \times 10^5$ plaque forming units (PFU) of infectious rVSV–eGFP–SARS-CoV-2 (muliplicity of infection [MOI] = 0.5) for long-term infection assays or for 48 hours before live confocal imaging.

For long-term organoid viral quantification experiments, 75,000 Barrett's esophagus cells were seeded into 48-well plates before viral infections as described. Brightfield and fluorescent imaging was performed using the BioTek Lionheart Cell Imaging Multimode Reader as described below every 12 hours for 312 hours total or every day for 14 days. Visible green punctate per well was counted for Experiment 1, and visible green puncta in organoids larger than 10 $\mu$m were counted for Experiment 2. These data were then graphed and analyzed using GraphPad Prism 8.1.1. For statistical analysis that incorporated the repeated, sequential measures of the same cultures over time, data were transformed by measuring the area under the curve for each time point until day 5 (the time point in both

experiments when peak viral entry returned toward a steady-state, baseline in all organoid lines). Statistical significance was calculated from the transformed data (ie, the area under the curve calculations). For the 2 organoid lines in Experiment 1, a paired 2-tailed Student's *t* test was used. Statistical significance for Experiment 2 was calculated using paired analysis of variance of mean area under the curve values with post hoc Dunnett correction where WU012 was considered the control. Alpha was 0.05 for all approaches.

### *Imaging*

Fluorescence microscopy was performed using a Zeiss Axiovert 200 microscope with an Axiocam MRM camera and Apotome II instrument for grid-based optical sectioning. Immunofluorescence images were taken on a Zeiss Apotome. Brightfield images were taken on an Olympus BX43 light microscope. Long-term infection organoid fluorescent imaging was performed on a BioTek Lionheart Cell Imaging Multimode Reader. Live confocal imaging was performed at the Washington University Center for Cellular Imaging using a Zeiss LSM880 Confocal Microscope with Airyscan unit and Pecon stage-top incubator. Images were analyzed and postimaging adjustments were performed with Adobe Photoshop CS6, and line art was generated in Adobe Illustrator CS6.

## References

1. VanDussen KL, S, et al. Stem Cell Res 2019;37:101430.
2. Sato T, et al. Gastroenterology 2011;141:1762–1772.
3. Case JB, et al. Cell Host Microbe 2020;28:475–485.
4. Whelan SP, et al. Proc Natl Acad Sci USA 1995;92:8388–8392.

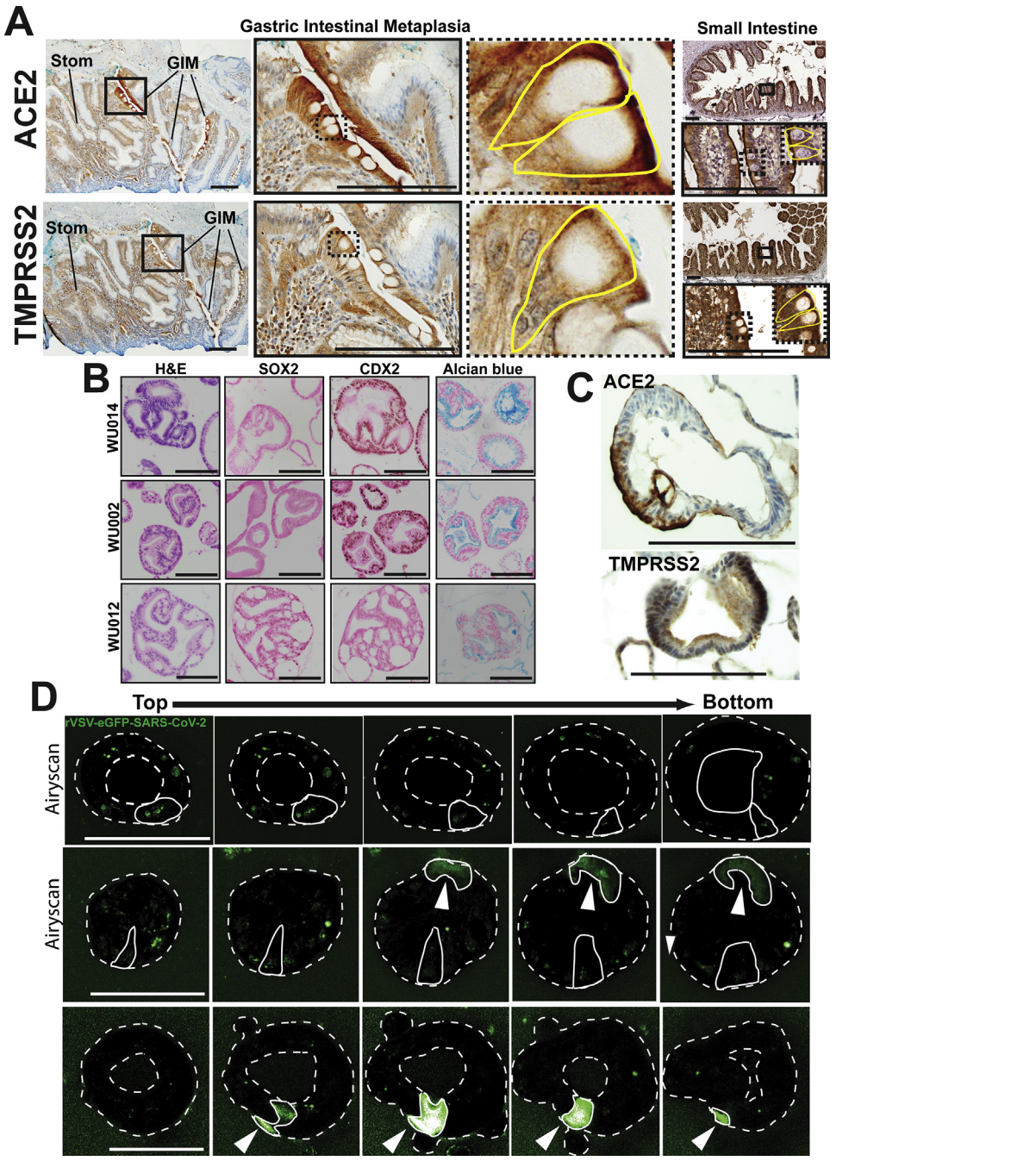


**Supplementary Figure 1.** Gastric intestinal metaplasia expresses ACE-2 and TMPRSS2; additional characterization of Barrett's esophagus organoids. (*A*) Immunohistochemistry of human gastric intestinal metaplasia (*GIM*) and adjacent stomach (*Stom*) shows apical expression of ACE-2 and TMPRSS2. Small intestine staining for both proteins shown as a positive control. Insets highlight individual goblet cells outlined in *yellow* with apical ACE-2 and TMPRSS2 expression patterns. Scale bars, 200 $\mu$m. (*B*) Hematoxylin and eosin images demonstrating the distinct columnar epithelium morphology and immunohistochemical staining of SOX2 (*brown* nuclear pattern), CDX2 (*brown* nuclear pattern), and Alcian blue (*blue* vesicular cytoplasmic pattern) for 3 human Barrett's esophagus organoid lines (WU014, WU002, and WU012). Scale bars, 100 $\mu$m. (*C*) Immunohistochemical staining of ACE-2 (*brown* apical cytoplasmic) and TMPRSS2 (*brown* diffuse cytoplasmic) for the intestinal WU002 human Barrett's esophagus organoid line. Scale bars, 100 $\mu$m. (*D*) Three-dimensional confocal Z-stack series ("top" of the organoid to the "bottom") with Airyscan detector used as indicated of live Barrett's organoids infected with rVSV–eGFP–SARS-CoV-2 demonstrating diffuse cytoplasmic (*arrowheads*) and punctate vesicular green GFP patterns. The organoid lumen and outer surface are marked by a *dotted line*. As an example, individual infected cells are outlined with a *solid line* in each organoid. Individual green infected cells are outlined with a *solid line* in each organoid showing diffuse cytoplasmic (*arrowheads*) and punctate vesicular GFP patterns. Scale bars, 100 $\mu$m.

| Age | Sex | PPI Use | Biopsy Location | Diagnosis | ACE2 Score (Metaplasia) | ACE2 Score (Adjacent Tissue) | TMPRSS2 Score (Metaplasia) | TMPRSS2 Score (Adjacent Tissue) |
|---|---|---|---|---|---|---|---|---|
| 57 | M | Yes | Esophagus | Barrett's without dysplasia | 1 | 0 | 1 | 0 |
| 82 | M | Yes | Esophagus | Barrett's without dysplasia | 2 | 0 | 1 | 0 |
| 63 | M | No | Esophagus | Barrett's without dysplasia | 2 | 0 | 1 | 0 |
| 78 | M | Yes | Esophagus | Barrett's without dysplasia | 1 | 1 | 1 | 0 |
| 75 | M | Yes | GE Junction | Barrett's without dysplasia | 2 | 0 | 1 | 0 |
| 76 | M | Yes | Esophagus | Barrett's without dysplasia | 1 | 0 | 1 | 0 |
| 60 | F | Yes | GE Junction | Barrett's without dysplasia | 1 | 0 | 2 | 0 |
| 57 | M | Yes | Esophagus | Barrett's without dysplasia | 2 | N/A | 1 | N/A |
| 66 | M | Yes | Esophagus | Barrett's without dysplasia | 2 | 0 | 0 | 0 |
| 68 | M | No | Esophagus | Barrett's without dysplasia | 2 | 0 | 1 | 0 |
| 59 | M | No | Esophagus | Barrett's without dysplasia | 2 | 0 | 1 | 0 |
| 71 | M | Yes | Esophagus | Barrett's without dysplasia | 2 | 0 | 1 | 0 |
| 75 | M | Yes | GE Junction | Barrett's without dysplasia | 2 | 0 | 1 | 0 |
| 66 | M | Yes | Esophagus | Barrett's with Low-grade dysplasia | 2 | N/A | 1 | N/A |
| 84 | M | Yes | Esophagus | Barrett's with Low-grade dysplasia | 2 | 0 | 1 | 0 |
| 66 | M | Yes | Esophagus | Barrett's with Low-grade dysplasia | 2 | 0 | 2 | 0 |
| 54 | F | Yes | Esophagus | Barrett's with High-grade dysplasia | 2 | 0 | 1 | 0 |
| 67 | M | Yes | Esophagus | Barrett's with High-grade dysplasia | 2 | 0 | 2 | 0 |
| 71 | M | No | Esophagus | Barrett's with High-grade dysplasia | 2 | 0 | 1 | 0 |
| 60 | M | No | Esophagus | Barrett's with High-grade dysplasia | 1 | 0 | 1 | 0 |
| 53 | M | Yes | GE Junction | Barrett's with High-grade dysplasia | 2 | 0 | 2 | 0 |
| 60 | F | Yes | GE Junction | Barrett's with High-grade dysplasia | 2 | 0 | 2 | 0 |
| 78 | M | Yes | Esophagus | Barrett's with High-grade dysplasia | 2 | 0 | 1 | 0 |
| 60 | F | No | Esophagus | Barrett's with High-grade dysplasia | 2 | 0 | 1 | 0 |
| 65 | M | No | Esophagus | Barrett's with High-grade dysplasia | 2 | 0 | 1 | 0 |
| 51 | M | No | Esophagus | Barrett's with High-grade dysplasia | 2 | 0 | 2 | 0 |
| 54 | M | Yes | Gastric | Intestinal Metaplasia | 1 | 0 | 0 | 0 |
| 49 | F | No | Gastric | Intestinal Metaplasia | 2 | 0 | 1 | 0 |
| 73 | M | Yes | Gastric | Intestinal Metaplasia | 2 | N/A | 1 | N/A |
| 76 | M | Yes | Gastric | Intestinal Metaplasia | 2 | 0 | 1 | 0 |
| 69 | M | No | Gastric | Intestinal Metaplasia | 1 | 0 | 1 | 0 |

**Supplementary Table 1.** Barrett's esophagus and gastric intestinal metaplasia express ACE-2 and TMPRSS2. Patient age, sex, protein pump inhibitor (PPI) use, biopsy location (esophagus, gastroesophageal junction, stomach), pathologic diagnosis, and quantification of ACE-2 and TMPRSS2 immunohistochemical staining in human tissue specimens of Barrett's esophagus (Barrett's without dysplasia, Barrett's with low-grade dysplasia, Barrett's with high-grade dysplasia) and gastric intestinal metaplasia. Scoring system: 0 = no apical staining; 1 = <50% of apical staining, 2 = >50% apical staining in 20× fields of view in areas of Barrett's esophagus or gastric intestinal metaplasia and adjacent tissue controls. N/A, areas without adjacent tissue controls.